Small Extracellular Vesicles Derived From Human Ipsc-Derived MSC Ameliorate Tendinopathy-Related Acute Pain Through Inhibiting Mast Cells Activation

Renzhi Gao
Shanghai Jiao Tong University Affiliated Sixth People' Hospitaliated to Shanghai Jiaotong University
Teng Ye
Shanghai Jiao Tong University Affiliated Sixth People' Hospitaliated to Shanghai Jiaotong University
Zhaochen Zhu
Shanghai Jiao Tong University Affiliated Sixth People' Hospitaliated to Shanghai Jiaotong University
Qing Li
Shanghai Jiao Tong University Affiliated Sixth People' Hospitaliated to Shanghai Jiaotong University
Juntao Zhang
Shanghai Jiao Tong University Affiliated Sixth People' Hospitaliated to Shanghai Jiaotong University
Ji Yuan
Shanghai Jiao Tong University Affiliated Sixth People' Hospitaliated to Shanghai Jiaotong University
Bizeng Zhao
Shanghai Jiao Tong University Affiliated Sixth People' Hospital
Zongping Xie (x91034@qq.com)
Shanghai Jiao Tong University Affiliated Sixth People' Hospital
Yang Wang
Shanghai Jiao Tong University Affiliated Sixth People' Hospitaliated to Shanghai Jiaotong University

Research Article

Keywords: iMSC-sEVs, tendinopathy, pain, mast cell

Posted Date: December 6th, 2021

DOI: https://doi.org/10.21203/rs.3.rs-1130900/v1

Abstract

Background: Acute pain is the primary symptom of tendinopathy, and mast cells activation is a nonnegligible cause. Currently, safe and effective treatment for acute pain in tendinopathy is still lacking. This study was aimed to explore the analgesic effect of iPSC-derived mesenchymal stem cell-derived small extracellular vesicles (iMSC-sEVs) on acute pain and further investigate the underlying mechanisms in tendinopathy.

Methods: A rat tendinopathy model was established and then treated with iMSC-sEVs or PBS for 4 weeks. The pathology of tendinopathy was accessed by H&E staining and immunohistochemical analysis 2 and 4 weeks after treatment. Then we measured pain-related behaviors 4 weeks after treatment. Double immunofluorescent staining on tendon sections for tryptase and PGP9.5 was conducted to assess whether iMSC-sEVs inhibit mast cells activation in tendinopathy. To further investigate the potential mechanism, RBL-2H3 cells were stimulated with substance P to mimic tendinopathy condition in vitro. The effect of iMSC-sEVs on inhibiting mast cells activation was measured by b-Hexosaminidase release assay, RT-qPCR, Toluidine blue staining and ELISA. RNA-seq was performed to analyze the related global changes and discover the underlying mechanism.

Results: iMSC-sEVs effectively reduced inflammation, thereby alleviating acute pain in tendinopathy as reflected by histological analysis and pain-related behaviors. Moreover, iMSC-sEVs inhibited activated mast cell infiltration and interactions with nerve fibers in tendinopathy. In vitro study showed that the expression of proinflammatory cytokines and the degranulation of mast cells induced by substance P were reduced upon iMSC-sEVs treatment. Transcriptome analysis revealed that iMSC-sEVs treatment down-regulated the expression of genes involved in the HIF-1 signaling pathway.

Conclusion: Overall, this study demonstrated that iMSC-sEVs relieved tendinopathy-related pain through inhibiting mast cells activation partly via the HIF-1 signaling pathway. These findings provide a novel treatment strategy for pain derived from tendinopathy and unravel the molecular mechanism underlying the application of iMSC-sEVs on mast cells.

Background

Pain is defined as an unpleasant sensory and emotional experience of actual or potential tissue damage or an experience expressed in such terms(1), which can be acute or chronic. Persistent stimulation by acute pain would cause neural plasticity remodeling in pain coding pathways and develop into chronic pain(2). Thus, the key to preventing chronic pain is to control the progression of pain during the acute phase. Tendinopathy is a prevalent musculoskeletal disease characterized by pain, swelling, and limited joint movement(3). It was reported that the prevalence and incidence rates of lower extremity tendinopathy were 11.83 and 10.52 per 1000 person-years(4). Chronic pain derived from tendinopathy would limit the movements of joints, even resulting in disability. To date, most studies related to tendinopathy focus on promoting tendon regeneration without considering relieving acute pain. Clinically, the effectiveness of current treatments for acute pain in tendinopathy remains ambiguous. Though

corticosteroid injection has been a mainstay treatment for tendon-related disorders for many years, its effectiveness remains controversial(5). In conclusion, it is essential to explore a new therapeutic strategy to relieve acute pain derived from tendinopathy.

Mesenchymal stem cells (MSCs) have been well investigated in regulating immune response and tissue regeneration(6, 7). Recently, we have generated MSCs from induced pluripotent stem cells (iPSCs)(8). The MSCs derived from iPSCs (iMSCs) have a more robust proliferation and differentiation potential than adult BM-MSCs(9). Accumulating studies have indicated that the efficacy of MSCs is attributed to the paracrined small extracellular vesicles (sEVs), lipid bilayer nanoparticles containing proteins, lipids, nucleic acid, and other biomolecules(10, 11). Our previous research has shown that sEVs derived from iMSCs (iMSC-sEVs) could attenuate osteoarthritis by alleviating inflammation and promoting chondrocyte proliferation(12, 13). Besides, previous studies have demonstrated that BMSC-EVs could promote tendon healing by suppressing inflammation and apoptotic cell accumulation and increasing the proportion of tendon-resident stem/progenitor cells(14, 15). Nevertheless, the therapeutic potential of iMSC-sEVs for alleviating acute pain in tendinopathy has barely been reported so far.

As proinflammatory cells and the immune system's first responders (16), mast cells are localized in proximity to afferent fibers(17). The proximity of mast cells to afferent nerve fibers potentiates critical molecular crosstalk, contributing to initiating and developing pain responses(18). They are a critical link between the nervous system and the immune system(19). Studies have shown that mast cells play a vital role in pain transmission in tendinopathy(20–24), indicating that suppressing the infiltration and activation of mast cells may be a target for relieving acute pain in tendinopathy. In addition, Cho et al. reported that sEVs from human adipose tissue-derived MSCs could ameliorate atopic dermatitis and reduce the infiltration of mast cells in vivo(25). Liu et al. showed that human MSC-derived sEVs prevented the rupture of intracranial aneurysm, in part due to their anti-inflammatory effect on mast cells(26). Accordingly, we hypothesized that iMSC-sEVs could ameliorate pain by inhibiting mast cell activation in tendinopathy.

In the present study, we first found that iMSC-sEVs could relieve acute pain and inhibit inflammation in a rat tendinopathy model. Then we showed that iMSCs-sEVs could inhibit mast cells activation and interaction with nerve fibers in vivo. Moreover, iMSC-sEVs inhibited substance P-induced activation of mast cells in vitro. Mechanically, iMSC-sEVs might regulate the HIF-1 signaling pathway in mast cells. Herein, we demonstrated for the first time that iMSC-sEVs possess the therapeutic potential to ameliorate pain in tendinopathy by stabilizing mast cells, at least in part, via the HIF-1 signaling pathway.

Methods

Derivation and characterization of induced MSCs

The local ethics committee approved using human iPSC in this study of the Shanghai Sixth People's Hospital affiliated with Shanghai Jiao Tong University. The generation of mesenchymal stem cells from

human induced pluripotent stem cells as previously described (27). Flow cytometry was used to detect phenotypical markers of iMSCs. The cells were incubated with 1% (w/v) bovine serum albumin (BSA) (Gibco) to block the non-specific antigens. Then, 1×10^6 cells were stained with the following conjugated mouse monoclonal antibodies: CD24-PE (1:100, 560991, BD Biosciences), CD29-PE (1:100, 561795, BD Biosciences), CD44-FITC (1:100, 560977, BD Biosciences), CD146-PE (1:100, 561013, BD Biosciences), CD133-PE (1:100, 130080081, MACS), CD105-FITC (1:100, 560943, BD Biosciences), CD73-PE (1: 100, 561014, BD Biosciences), CD90-PE (1:100, 328109, Biolegend), CD34-APC (1: 100, 560940, BD Biosciences), CD45-FITC (1:100, 560976, BD Biosciences), and HLA-DR-PE (1:100, 560943, BD Biosciences). After being washed in 1% (w/v) BSA twice, the cells were resuspended in 1% BSA and analyzed by CytoFLEX flow cytometer (Beckman Coulter Life Science, USA).

Isolation of iMSC-sEV

The iMSC-sEV were isolated from the cell culture medium of iMSCs by differential ultracentrifugation protocols. Briefly, the obtained medium was centrifuged at 300g for 10 min and 2000g for 10 min. After centrifugation at 10,000g for 1 h, the supernatant was filtered through a 0.22-μm filter sterilize Steritop™ (Millipore) to remove cellular debris and microvesicles. The collected medium was further ultracentrifuged at 100,000g for 70 min twice. After removal of the supernatant, the pellet was resuspended in PBS.

Size distribution and particle concentration of iMSC-sEVs

The size and concentration of the iMSC-sEVs were assessed using nano-flow cytometer (N30 Nanoflow Analyzer, NanoFCM Inc., Xiamen, China) as previously described(28). Briefly, isolated iMSC-sEVs diluted with 100-fold PBS (for a nanoparticle concentration of approximately 10^8/mL) were loaded to the nano-flow to measure the side scatter intensity (SSI). The concentration of iMSC-sEVs was calculated according to the ratio of SSI to particle concentration in the standard polystyrene nanoparticles. The size distribution of iMSC-sEVs sample was calculated according to the standard cure generated by standard silica nanoparticles.

Western blot analysis

To identify sEV using western blot analysis, three positive markers of iMSC-sEV, including CD9, TSG101, and CD63, and one negative marker GM130, were evaluated. Cells or iMSC-sEV proteins were harvested using RIPA lysis buffer (Beyotime biotechnology, China, P0013C) supplemented with protease inhibitor cocktail (Beyotime biotechnology, China, ST505). Lysates were cleared by centrifugation at 12,000 g for 20 min. The supernatant fractions were used for western blot analysis. Protein extracts were resolved by 10% SDS-PAGE and probed with the indicated antibodies. The antibodies against the following proteins were used for western blot analysis: rabbit monoclonal anti-CD9 (1:1000, Cell Signaling Technology, USA, 13174 s), mouse monoclonal anti-TSG-101 (1: 1000, Abcam, UK, ab83), Rabbit monoclonal anti-CD63 (1:1000, Abcam, UK, ab134045), and mouse polyclonal anti-GM130 (1:500, Abcam, UK, ab169276). Anti-rabbit IgG or anti-mouse IgG, HRP-linked antibody (1: 2,000; Cell Signaling Technology) was used as the secondary antibody. Protein level was detected using the ECL detection system.

Animal model and experimental design

Animal care and experimental procedures were approved by the Animal Research Committee of the Shanghai Jiao Tong University Affiliated Sixth People's Hospital (approval code: DWLL2021-0910). Previous studies have established a rat tendinopathy model by carrageenan(29). Hence, we injected 100ul 4% (w/v) carrageenan into the peritendon space of the quadriceps tendon under ultrasound guidance to induce a rat tendinopathy model while sham rats received a PBS injection. One week later, injection of iMSC-sEVs was performed in the sEVs group and PBS in the control group once a week for 4 weeks. Pain-related behaviors were analyzed one week after the administration of iMSC-sEVs or PBS. Reversal (%) of pain-related behaviors was calculated as follows:

$$Reversal(\%) = 100 \times \frac{(\mathrm{posttreatvalue, tendinopathyrats}) - (\mathrm{pretreatvalue, tendinopathyrats})}{(\mathrm{avg.\ pretreatvalueshamrats}) - (\mathrm{pretreatvalueintendinopathyrats})}$$

where "value" represents the values for static weight-bearing or hind paw withdrawal threshold.

Pain assessment

Hind-Paw Withdrawal Threshold

Hind-paw withdrawal thresholds were measured as described previously(30). The electronic von Frey instrument (model BIO-EVF4; Bioseb, Vitrolles France) was used to vertically stimulate the center of the rat hind paw with increasing intensity. The probe tip was gently placed perpendicularly into the mid-plantar surface of the paw, and steadily increasing pressure was applied until the hind paw was first lifted. Until the withdrawal reaction was positive, and there were 3 positive withdrawal reactions within the 5 consecutive stimuli, the value was defined as PWT and was expressed in grams (g).

Static Weight Bearing

The static weight-bearing (SWB) distribution over the right and left knee was assessed by measuring the postural balance between the injected and non-injected leg (30). Briefly, a rat was placed in the chamber of a weight-bearing measuring device (model #BIO-SWB-TOUCH-M; Bioseb). The force applied through each hind limb to the paw resting on the floor of the chamber was measured in grams (g), and an SWB index was calculated as follows:

$$SWBindex = \frac{\mathrm{Forceappliedtorightlimb}}{\mathrm{Forceappliedtorightlimb} + \mathrm{Forceappliedtoleftlimb}}$$

For each rat, the test was given at least three times at each assessment period.

Gait analysis

Dynamic pain-related behavior was measured by the gait of the rats(31). The Catwalk system objectively quantifies behavioral gait adaptation after daily use of a painful limb, automatically documenting paw placements on a surface and related parameters of inter-limb coordination(32). Briefly, rats were placed on a walkway apparatus (Shanghai Mobiledatum Information Technology, Shanghai, China). A camera below the walkway captures and digitally records footprint images. These paw print placements and gait

parameters were collected and further analyzed by WalkAnalysator (Shanghai Mobiledatum Information Technology). The CatWalk gait test was administered at weeks 4 after treatment. Print area, swing speed, duty cycle and max contact mean intensity were recorded and analyzed as Right/Left.

Histology and Immunohistochemistry

For histological analysis, the rat tendon samples were fixed en bloc in 4% PFA for 24 hours, dehydrated with a graded ethanol series, embedded in paraffin, and sectioned (5 μm thick) parallel to the long axis of the tendon. The sections were prepared for hematoxylin and eosin (H&E) and immunohistochemical analysis.

To assess the proinflammatory cytokine distribution in rat tendon samples, we performed immunohistochemistry (IHC) staining on paraffin-embedded sections. The following antibodies were used: anti-interleukin-1β (IL-1β) (1:500, Abcam, UK, ab283818), anti-tumor necrosis factor-α (TNF-α) (1:500, Abcam, UK, ab217706), anti-interleukin-6 (IL-6) (1:500, Abcam, UK, ab ab9324), and anti-nerve growth factor (NGF) (1:500, Abcam, UK, ab52987). HRP-conjugated antibodies were used with DAB as the chromogen for visualization. In some cases, a hematoxylin counterstaining was done for nuclear counterstaining. Histological and immunohistochemical staining was evaluated and photo-documented digitally with the microscope (Leica, DM6B, Germany). Interpretation of the slides was performed by semi-quantitative grading scale of Movin score for tendon abnormalities(33).

Immunofluorescence staining

The rats were sacrificed, and cardiac perfusion was performed with ice-cold saline, followed by 4% (w/v)paraformaldehyde perfusion. Lumbar dorsal root ganglion (DRG) at levels L3–L5 and tendon tissues were dissected from the surrounding tissue, fixed in 4% formaldehyde overnight at 4°C, and dehydrated with gradient sucrose solutions (20%, 30%, and 35% (w/v)). After being embedded and frozen in an optimal cutting temperature compound (OCT), the tissues were sliced into 10-μm-thick coronal sections. The sections were then stained with specific markers, including calcitonin gene-related peptide (CGRP, 1:400, Cell Signaling Technology, 14959), iNOS (1:400, Cell Signaling Technology, 13120), Tryptase (1:100, Abcam, UK, ab2378) and PGP9.5(1:100, Abcam, UK, ab108986). Fluorescence images were acquired using a fluorescence microscope (Leica, DM6B, Germany). ImageJ software (National Institutes of Health, Bethesda, MD, USA) was performed to quantify Tryptase+ cell number, staining area, and relative expression of CGRP and iNOS.

Uptake of iMSC-sEVs by mast cells in vitro

To determine the uptake of iMSC-sEVs into RBL-2H3 cells in vitro, we labeled iMSC-sEVs with Dil fluorochrome (Thermo Fisher, USA) under room temperature for 15 min, followed by ultracentrifugation at 100,000g in PBS to get rid of the unlabeled dye. Next, Dil-labeled sEV were incubated with RBL-2H3 cells for 12 hours. And then, the culture medium was discarded, and the cells were rinsed twice with PBS before image capture under the fluorescence microscope (Leica, DM6B, Germany).

SP-induced degranulation in RBL-2H3 cells

RBL-2H3 cells were kindly provided by Stem Cell Bank, Chinese Academy of Sciences. The cells were grown in Eagles Modified Essential Medium (EMEM) supplemented with glutamine (2 mM), penicillin (50 U/ml), streptomycin (50 μg/ml), and 10% fetal bovine serum (FBS, Gibco), in a humidified 5% CO2 atmosphere at 37°C, plated on 6-well culture dishes at a cell density of 9 × 105 cells per well, at 37°C in 5% CO_2 atmosphere. After 24 hours, RBL- 2H3 cells were stimulated with SP (10 μM) or vehicle (PBS) and incubated for 15 min at 37°C in 5% CO2 atmosphere.

β-Hexosaminidase release assay

The RBL-2H3 cells were conducted β-Hexosaminidase release assay as previously described with a small modification to determine the degranulation activity(34). Briefly, after being stimulated by SP, the RBL-2H3 cells were treated with iMSC-sEVs (10^9/ml) or vehicle for different time (6h/ 9h/ 12h/ 24h) at 37°C in 5% CO2 atmosphere. The supernatants (15 μl) were incubated with 60 μl of the substrate (1 mM p-nitrophenyl-N-acetyl-β-D-glucosaminide in citrate 0.05 M, pH 4.5) for 1 h at 37°C. Furthermore, the cells were lysed with 0.1% Triton X-100 and incubated with the substrate to determine the degranulation activity in the supernatants to determine the total amount of released β-hexosaminidase. The reaction was stopped by 150 μl of 0.1 M sodium bicarbonate buffer (pH 10.0), and the reaction product was monitored by measuring the optical density (OD) at 405 nm by using a reader GENios Pro (Tecan). The results were calculated by using the following formula: % degranulation = [OD-supernatant/(OD-supernatant + OD-triton x−100)] × 100.

Real-time quantitative polymerase chain reaction (RT-qPCR) analysis

The expression of targeted genes was analyzed by RT-qPCR. Briefly, The total RNA of samples was extracted using EZ-press RNA Purification Kit (EZBioscience, USA). RNA quantity and purity were confirmed with a Nanodrop spectrophotometer (Thermo Scientific, Wilmington, DE). A 4× Reverse Transcription Master Mix (EZBioscience, USA) was used for reverse transcription reaction. PCR reactions were run using the ABI Prism 7900HT Real-Time System (Applied Biosystems, Carlsbad, CA) with 2× SYBR Green qPCR Master Mix (EZBioscience, USA). The primer sequences used in this study are listed in Additional file 1: Table S1.

Additional file 1: Table S1. The primer sequences were used in this study.

Enzyme-linked Immunosorbent Assays (ELISA)

The supernatant collected at 18h after different treatment was evaluated for proinflammatory molecules and NGF by ELISA. IL-1β, TNF-α, IL-6, IL-10, and NGF concentrations were measured by using a rat ELISA kit (Shanghai Westang Bio-Tech Co., LTD., Shanghai, China) according to the manufacturer's instructions. The absorbance was measured by a microplate reader (Thermo Fisher Scientific, Waltham, MA, USA) at 450 nm.

Statistical analysis

Data were presented as mean ± SD. Student t-test was used to assess the difference between two groups, and the one-way ANOVA with the Bonferroni post hoc test was applied for comparisons among multiple groups. All experiments were independently performed at least three times. Statistical analysis was performed using GraphPad Prism software (version 8.0). The significant difference was considered to be *P*-value < 0. 05.

Results

Characterization of iMSCs and iMSC-sEVs

First, flow cytometry was applied to evaluate the cell surface antigen profile of iMSCs. The results showed that iMSCs highly expressed antigen markers, including CD73, CD105, CD90, CD29, CD146 and CD105, but not CD34, CD45, CD133 and HLA-DR (Fig. 1A). iMSC-sEVs were isolated from the cell culture supernatant of iMSCs and identified using transmission electron microscope (TEM), nano-flow cytometer, and western blot analysis. TEM showed that iMSC-sEVs were typical cup-shaped vesicles (Fig. 1B). Nano-flow cytometer analysis revealed that the average diameter was ranged from 50 to 200 nm, and the concentration of the iMSC-sEV was approximately 1.6×10^{10} particles/mL (Fig. 1C). Western blot analysis determined the presence of exosomal markers CD9, TSG101, and CD63, whereas the cis-Golgi matrix protein GM130 was not detected (Fig. 1D). As shown in Fig. 1E-F, the mean particle concentration was $0.62 \times 10^{8} \pm 0.09 \times 10^{8}$ particles/ mL conditioned medium (CM), or 420.20 ± 61.01 particles per cell (Fig. 1E). The mean protein concentration was 6102.39 ± 190.29 ng/mL CM, or $100.32 \times 10^{-6} \pm 13.56 \times 10^{-6}$ ng per particle (Fig. 1F).

iMSC-sEVs alleviated the tendinopathy-related pain in a rat model

Firstly, we established the tendinopathy model by injecting carrageenan into the quadriceps tendon, and then iMSC-sEVs (1×10^{9} particles) or PBS were administrated. (see Additional file 2: Fig. S1). Then, we performed H&E and IHC staining on the quadriceps tendon. H&E staining revealed that tendons in the iMSC-sEVs group showed more continuous and regular arrangement than disorganized tendons in the vehicle group (Fig. 2A). Besides, Movin score in the iMSC-sEVs group was significantly lower than the vehicle group (Fig. 2B). IHC staining showed that proinflammatory cytokine expression significantly decreased in the iMSC-sEVs group compared with the vehicle group at 2 weeks and 4 weeks (Fig. 2A, 2B). Our results suggested that iMSC-sEVs could reduce proinflammatory cytokines production and repair the injured tendon.

Pain is a dominant character of inflammation. Therefore, we evaluated whether iMSC-sEVs could relieve the pain in tendinopathy. We accessed static weight-bearing (SWB) and hind-paw withdrawal threshold (PWT) after iMSC-sEVs administration for 4 weeks. For the static state, the reversals(%) of PWT and SWB in the iMSC-sEVs group were significantly increased compared to the vehicle group (Fig. 2C, D). CatWalk tests were applied to examine whether iMSC-sEVs improve gait and motor function at 4 weeks after treatment. The lower limbs of the vehicle group showed less coordination than that of the iMSC-sEVs

treatment group during walking (Fig. 2E). Specifically, iMSC-sEVs significantly elevated the right /left hind values ratio in the print area, swing speed, and max contact mean intensity compared with the vehicle group (Fig. 2F). In addition, He et al. reported that BMSC-sEVs could reduce the expressions of CGRP (neuropathic pain marker) and iNOS (inflammatory marker) in OA rats' dorsal root ganglion (DRG) tissues(35). Therefore, we performed immunofluorescence staining to detect the expressions of CGRP and iNOS. The result showed that the expression of these two proteins was significantly downregulated in DRG of the iMSC-sEVs group compared with the vehicle group (see Additional file 3: Fig. S2A, B). These results indicated that iMSC-sEVs could mitigate tendinopathy-related pain.

iMSC-sEVs inhibited mast cells infiltration and interactions with nerve fibers in the quadriceps tendon

Previous reports have demonstrated that mast cells play a vital role in tendinopathy-related pain(20–23). We conducted double immunofluorescence staining on tendon sections for tryptase and PGP9.5 to assess the number of activated (tryptase+) mast cells and the anatomical interaction between mast cells and nerve fibers. The results showed that compared to the sham group, tryptase+ mast cells increased markedly in the tendinopathy group, as evidenced by the mean gray value of the tryptase staining area (Fig. 3A, B). Besides, the number of tryptase+ mast cells closed (≤5 μm) to PGP9.5+ nerve fibers significantly also increased (Fig. 3A, B).

It is well known that NGF is a prominent role that mediates interactions among mast cells and nerve fibers(36). As expected, IHC staining of NGF showed a significantly increased expression compared to the sham group (Fig. 3C, D). Therefore, these data supported the assumption that enhanced activation of mast cells after model establishment.

We then investigated whether iMSC-sEVs could regulate activated mast cells infiltration and interaction with nerve fibers. Double immunofluorescence staining for tryptase and PGP9.5 was applied as described above. Compared with vehicle treatment, iMSC-sEV treatment significantly reduced the infiltration and interaction, as reflected by the significantly decreased number of tryptase+ mast cells and that near PGP9.5+ nerve fibers (Fig. 3A, B). Additionally, iMSC-sEV treatment significantly decreased the positive area of NGF compared to vehicle treatment (Fig. 3C, D). Altogether, these results suggested that iMSC-sEVs treatment could stabilize mast cells under inflammatory conditions and impede their crosstalk with nerve fibers in a tendinopathy model.

iMSC-sEVs restrained Substance P-induced activation of mast cells

To further investigate the effect of iMSC-sEVs on the function of mast cells, substance P (SP) was applied to activate RBL-2H3 cells (a widely used mast cell line(37)) in vitro. First of all, we determined whether iMSC-sEVs could be internalized by RBL-2H3 cells. iMSC-sEVs were labeled with Dil fluorescent dye and added to the culture medium. After 12 h of incubation, Dil-labeled iMSC-sEVs were efficiently up-taken by RBL-2H3 cells (Fig. 4A). RT-qPCR results showed that iMSC-sEVs reduced the mRNA expression of IL-1β, IL-6, TNF-α and NGF from SP-stimulated RBL-2H3 cells in a dose-dependent manner (Fig. 4B). Therefore, iMSC-sEVs with the dose of 1×10^9 particles/ml were chosen for the following experiments. β-

hexosaminidase release assay showed that iMSC-sEVs significantly reduced the degranulation of SP-stimulated RBL-2H3 cells, especially after 12 h incubation (Fig. 4C). Toluidine blue staining showed that iMSC-sEVs significantly reduced the percentage of degranulated mast cells compared with vehicle treatment (Fig. 4D, E). In addition, the expression of proinflammatory cytokines in the supernatant was significantly declined in the iMSC-sEVs group as determined by ELISA (Fig. 4F). Collectively, these data indicated that iMSC-sEVs restrained SP-induced activation of mast cells in vitro.

iMSC-sEVs modulated the gene expression pattern of mast cells

To elucidate the underlying molecular mechanism by which iMSC-sEVs restrained the degranulation of mast cells, we performed RNA-seq analysis to profile the gene expression patterns in SP-stimulated RBL-2H3 cells treated with vehicle and iMSC-sEVs. We identified 768 up-regulated genes (> 2-fold, $p < 0.05$) and 530 down-regulated genes (< 0.5-fold, $p < 0.05$) after iMSC-sEVs treatment (Fig. 5A, B). Moreover, Kyoto Encyclopedia of Genes and Genomes (KEGG) pathway analysis indicated that the downregulated genes in the iMSC-sEVs group were enriched for functional annotations related to the HIF-1 signaling pathway and other metabolic pathways (Figure. 5C). Similarly, Gene Ontology (GO) analysis revealed that the downregulated genes in the iMSC-sEVs group were enriched for biological processes, such as regulation of apoptotic cell clearance and positive regulation of IL−1β secretion and response to type I interferon (Fig. 5D). Subsequently, the heatmap verified the expression of specific genes in the HIF-1 signaling pathway analysis and biological processes like positive regulation of IL−1β and response to interferon, which showed a significant difference between groups (fold change >2) (Fig. 5E). Furthermore, RT-qPCR analysis confirmed that the expression of the HIF-1 signaling pathway-related genes was down-regulated after iMSC-sEVs treatment (Fig. 5F). Therefore, these results suggested that iMSC-sEVs restrained mast cell activation through regulating the HIF-1 signaling pathway.

Discussion

In this study, we demonstrated for the first time that the application of sEVs isolated from iPS-MSCs (iMSC-sEVs) significantly alleviated acute pain in a rat tendinopathy model. We found that iMSC-sEVs could notably inhibit mast cell activation and suppress inflammation in vivo. Further in vitro study illustrated that iMSC-sEVs could restrain SP-induced mast cells activation via the HIF-1 signaling pathway in part.

Tendinopathy describes a spectrum of changes in damaged and diseased tendons, resulting in pain and dysfunction(38). The pathogenesis of tendinopathy is multifactorial and complex. It is widely accepted that overuse and inflammation contribute to tendinopathy(39, 40). This study focused on the pathogenicity of inflammation. Pain is an essential manifestation of inflammation, but pain can generally be classified into nociceptive pain, inflammatory pain and neuropathic pain according to the pathogenesis. Nociceptive and inflammatory pain are adaptive and protective, while neuropathic pain occurs after damage to the nervous system. In tendinopathy, inflammatory mediators evoke pain via direct activation and sensitization of nociceptors(41). In contrast, persistent nociceptive input results in

the growth of central sensitization and neuropathic pain, characterized by the hyperactivity and hyperexcitability of neurons in the brain and spinal cord(42). Besides, previous studies suggest that tendinopathy-related pain is a combinational form of inflammatory and neuropathic pain(43, 44). Calcitonin gene related peptide (CGRP) is generally involved in transmitting nociceptive information and pain sensitization in the peripheral and spinal cords(35). Consistent with these, we determined the increased expression of CGRP and iNOS in dorsal root ganglion of tendinopathy rats. Meanwhile, iMSC-sEVs treatment relieved the pain in tendinopathy, thereby reducing central sensitization and neuropathic pain, as reflected by decreased expression of CGRP and iNOS.

After injuries occur in local tissue, mast cells and other immune cells are activated and release inflammatory mediators such as bradykinin, prostaglandin, protease and histamine to stimulate adjacent nociceptor afferent fibers(45, 46). In turn, affected afferent fibers of nociceptors also release neuromodulators, such as substance P (SP), calcitonin-producing peptide, and vasoactive intestinal protein to activate mast cells. Consequently, an inflammatory cascade reaction of mast cell activation and peripheral neuro-hypersensitivity is formed, further amplifying pain and inflammation(46–48) (49). Scott et al. revealed that the number of mast cells in the patellar tendon specimens of patients with patellar tendinopathy was significantly increased(21). Consistently, in this study, we found that the number of activated mast cells and those closed (≤5 μm) to PGP9.5+ nerve fibers significantly increased in the tendon after model establishment in rats. Therefore, mast cells may be a target for relieving acute pain in tendinopathy.

MSCs have been proved to possess anti-inflammatory, analgesic and regenerative capacities(50). However, current methods for the large-scale preparation of MSC face several limitations and challenges. MSCs derived from iPSCs (iMSCs) can avoid the ethical problem and immune rejection, and iMSC-sEVs production offers several advantages for applications of MSCs(11). The anti-inflammatory and analgesic effects of iMSCs are mediated by paracrine action, which is dominated by sEVs containing various nucleic acids, DNA, and proteins. Previous studies have reported that MSC-sEVs could inhibit mast cells activation via a PGE2-dependent mechanism(26). Our present research found that iMSC-sEVs dependently down-regulate SP-induced release of proinflammatory cytokines and degranulation of RBL-2H3 cells (a mast cell line(37)) in vitro. Besides, in vivo study showed that iMSC-sEVs decreased the expression of proinflammatory cytokines, the activation of mast cells and the distance with nerve fibers, confirming the ability of iMSC-sEVs in suppressing mast cells activation. As expected, our in vivo study showed that iMSC-sEVs treatment increased reversals(%) of PWT and SWB, improved gait performance and motor function, revealing the analgesic effect of iMSC-sEVs on tendinopathy in vivo. Overall, these results demonstrate that iMSC-sEVs alleviate pain derived from tendinopathy partially through inhibiting the activation of mast cells.

RNA-seq and bioinformatics analysis of sequencing data identified differentially expressed genes involved in several signaling pathways. Interestingly, the expression of genes in metabolism-related signaling pathways like glycolysis/gluconeogenesis, biosynthesis of amino acids, and carbon metabolism upregulated significantly in the vehicle group. It might be attributed to the activation of mast

cells caused by SP. So far, an increasing number of studies have reported that the HIF-1 signaling pathway figures prominently in regulating mast cells. Mast cells-derived HIF-1a significantly contributes to regulating mast cell function, which promotes the development of colorectal cancer(51). Abebayehu et al.(52) found that lactic acid could suppress IL-33-mediated mast cell inflammatory responses via HIF-1α-dependent miR-155 suppression. In addition, Yan et al.(53) discovered that SP could upregulate the level of HIF-1α in gingival fibroblasts and participate in periodontitis. According to the KEGG analysis, 17 genes in the HIF-1 signaling pathway downregulated significantly after iMSC-sEVs treatment and RT-qPCR confirmed it. Thus, our study suggests that iMSC-sEVs could module the activation and function of mast cells by regulating the HIF-1 signaling pathway.

Conclusions

In summary, our study report for the first time that iMSC-sEVs treatment relieves acute pain derived from carrageenan-induced rat tendinopathy by modulating neuro-immune interactions via the suppression of mast cells. Besides, iMSC-sEVs could suppress SP-stimulated activation in mast cells partly through regulating the HIF-1 signaling pathway. These findings unravel molecular mechanisms underlying the application of iMSC-sEVs on mast cells and provide a novel treatment strategy for pain derived from tendinopathy.

Abbreviations

iPSCs: Induced pluripotent stem cells; iMSCs: iPSCs-derived MSCs; iMSC-sEVs: iPSC-derived mesenchymal stem cell-derived small extracellular vesicles; BMSC-sEVs: Bone mesenchymal stem cell-derived small extracellular vesicles; HIF-1: Hypoxia inducible factor-1; PBS: Phosphate-buffered saline; PWT: Paw withdrawal thresholds; SWB: Static weight-bearing; H&E: Hematoxylin and eosin; IHC: Immunohistochemistry; IL-1b: Interleukin-1b; TNF-a: Tumor necrosis factor-a; IL-6: Interleukin-6; NGF: Nerve growth factor; iNOS: Inducible nitric oxide synthase; CGRP: Calcitonin gene-related peptide; SP: Substance P; OD: Optical density; RT-qPCR: Real-time quantitative polymerase chain reaction; ELISA: Enzyme-linked immunosorbent assays; TEM: Transmission electron microscope; PGP9.5: Protein gene product 9.5; KEGG: Kyoto encyclopedia of genes and genomes; GO: Gene ontology

Declarations

Acknowledgements

Thanks for all the support and contributions of participants.

Authors' contributions

GRZ and YT contributed to the cytology experiments, animal experiments, data acquisition, data analysis, and manuscript writing. ZZC, LQ, ZJT and YJ provided experimental technical support. ZBZ, XZP and WY took part in the experimental design and text revision. The authors read and approved the final manuscript.

Funding

This study was supported by the National Natural Science Foundation of China (81870972, 82072550).

Availability of data and materials

The data that support the findings of this study are available from the corresponding author upon reasonable request.

Ethics approval and consent to participate

Animal care and experimental procedures were approved by the Animal Research Committee of the Shanghai Jiao Tong University Affiliated Sixth People's Hospital (approval code: DWLL2021-0910).

Consent for publication

Not applicable

Competing interests

The authors declare that they have no conflicting interests.

References

1. Pain terms: a list with definitions and notes on usage. Recommended by the IASP Subcommittee on Taxonomy. Pain. 1979;6(3):249.
2. Matsuda M, Huh Y, Ji RR. Roles of inflammation, neurogenic inflammation, and neuroinflammation in pain. J Anesth. 2019;33(1):131–9.
3. Tang C, Chen Y, Huang J, Zhao K, Chen X, Yin Z, et al. The roles of inflammatory mediators and immunocytes in tendinopathy. J Orthop Translat. 2018;14:23–33.
4. Albers IS, Zwerver J, Diercks RL, Dekker JH, Van den Akker-Scheek I. Incidence and prevalence of lower extremity tendinopathy in a Dutch general practice population: a cross sectional study. BMC Musculoskelet Disord. 2016;17:16.
5. Irby A, Gutierrez J, Chamberlin C, Thomas SJ, Rosen AB. Clinical management of tendinopathy: A systematic review of systematic reviews evaluating the effectiveness of tendinopathy treatments. Scand J Med Sci Sports. 2020;30(10):1810–26.
6. Shi Y, Wang Y, Li Q, Liu K, Hou J, Shao C, et al. Immunoregulatory mechanisms of mesenchymal stem and stromal cells in inflammatory diseases. Nat Rev Nephrol. 2018;14(8):493–507.
7. Yang H, Feng R, Fu Q, Xu S, Hao X, Qiu Y, et al. Human induced pluripotent stem cell-derived mesenchymal stem cells promote healing via TNF-α-stimulated gene-6 in inflammatory bowel disease models. Cell Death Dis. 2019;10(10):718.
8. Hu GW, Li Q, Niu X, Hu B, Liu J, Zhou SM, et al. Exosomes secreted by human-induced pluripotent stem cell-derived mesenchymal stem cells attenuate limb ischemia by promoting angiogenesis in

mice. Stem Cell Res Ther. 2015;6(1):10.

9. Lian Q, Zhang Y, Zhang J, Zhang HK, Wu X, Zhang Y, et al. Functional mesenchymal stem cells derived from human induced pluripotent stem cells attenuate limb ischemia in mice. Circulation. 2010;121(9):1113–23.
10. Varderidou-Minasian S, Lorenowicz MJ. Mesenchymal stromal/stem cell-derived extracellular vesicles in tissue repair: challenges and opportunities. Theranostics. 2020;10(13):5979–97.
11. Park KS, Bandeira E, Shelke GV, Lässer C, Lötvall J. Enhancement of therapeutic potential of mesenchymal stem cell-derived extracellular vesicles. Stem Cell Res Ther. 2019;10(1):288.
12. Yang Y, Zhu Z, Gao R, Yuan J, Zhang J, Li H, et al. Controlled release of MSC-derived small extracellular vesicles by an injectable Diels-Alder crosslinked hyaluronic acid/PEG hydrogel for osteoarthritis improvement. Acta Biomater. 2021.
13. Zhu Y, Wang Y, Zhao B, Niu X, Hu B, Li Q, et al. Comparison of exosomes secreted by induced pluripotent stem cell-derived mesenchymal stem cells and synovial membrane-derived mesenchymal stem cells for the treatment of osteoarthritis. Stem Cell Res Ther. 2017;8(1):64.
14. Shi Z, Wang Q, Jiang D. Extracellular vesicles from bone marrow-derived multipotent mesenchymal stromal cells regulate inflammation and enhance tendon healing. J Transl Med. 2019;17(1):211.
15. Yu H, Cheng J, Shi W, Ren B, Zhao F, Shi Y, et al. Bone marrow mesenchymal stem cell-derived exosomes promote tendon regeneration by facilitating the proliferation and migration of endogenous tendon stem/progenitor cells. Acta Biomater. 2020;106:328–41.
16. Galli SJ, Nakae S, Tsai M. Mast cells in the development of adaptive immune responses. Nat Immunol. 2005;6(2):135–42.
17. Gupta K, Harvima IT. Mast cell-neural interactions contribute to pain and itch. Immunol Rev. 2018;282(1):168–87.
18. Morellini N, Finch PM, Goebel A, Drummond PD. Dermal nerve fibre and mast cell density, and proximity of mast cells to nerve fibres in the skin of patients with complex regional pain syndrome. Pain. 2018;159(10):2021–9.
19. Dothel G, Barbaro MR, Boudin H, Vasina V, Cremon C, Gargano L, et al. Nerve fiber outgrowth is increased in the intestinal mucosa of patients with irritable bowel syndrome. Gastroenterology. 2015;148(5):1002-11.e4.
20. Christensen J, Alfredson H, Andersson G. Protease-activated receptors in the Achilles tendon-a potential explanation for the excessive pain signalling in tendinopathy. Mol Pain. 2015;11:13.
21. Scott A, Lian Ø, Bahr R, Hart DA, Duronio V, Khan KM. Increased mast cell numbers in human patellar tendinosis: correlation with symptom duration and vascular hyperplasia. Br J Sports Med. 2008;42(9):753–7.
22. Behzad H, Sharma A, Mousavizadeh R, Lu A, Scott A. Mast cells exert proinflammatory effects of relevance to the pathophyisology of tendinopathy. Arthritis Res Ther. 2013;15(6):R184.

23. Alim MA, Ackermann PW, Eliasson P, Blomgran P, Kristiansson P, Pejler G, et al. Increased mast cell degranulation and co-localization of mast cells with the NMDA receptor-1 during healing after Achilles tendon rupture. Cell Tissue Res. 2017;370(3):451–60.
24. Dean BJ, Gettings P, Dakin SG, Carr AJ. Are inflammatory cells increased in painful human tendinopathy? A systematic review. Br J Sports Med. 2016;50(4):216–20.
25. Cho BS, Kim JO, Ha DH, Yi YW. Exosomes derived from human adipose tissue-derived mesenchymal stem cells alleviate atopic dermatitis. Stem Cell Res Ther. 2018;9(1):187.
26. Liu J, Kuwabara A, Kamio Y, Hu S, Park J, Hashimoto T, et al. Human Mesenchymal Stem Cell-Derived Microvesicles Prevent the Rupture of Intracranial Aneurysm in Part by Suppression of Mast Cell Activation via a PGE2-Dependent Mechanism. Stem Cells. 2016;34(12):2943–55.
27. Xia Y, Ling X, Hu G, Zhu Q, Zhang J, Li Q, et al. Small extracellular vesicles secreted by human iPSC-derived MSC enhance angiogenesis through inhibiting STAT3-dependent autophagy in ischemic stroke. Stem Cell Res Ther. 2020;11(1):313.
28. Tian Y, Ma L, Gong M, Su G, Zhu S, Zhang W, et al. Protein Profiling and Sizing of Extracellular Vesicles from Colorectal Cancer Patients via Flow Cytometry. ACS Nano. 2018;12(1):671–80.
29. Nf as J, Bartoaíková L. Carrageenan: a review. Vet Med (Praha). 2018;58:187–205.
30. Otis C, Gervais J, Guillot M, Gervais JA, Gauvin D, Péthel C, et al. Concurrent validity of different functional and neuroproteomic pain assessment methods in the rat osteoarthritis monosodium iodoacetate (MIA) model. Arthritis Res Ther. 2016;18:150.
31. Miyagi M, Ishikawa T, Kamoda H, Suzuki M, Sakuma Y, Orita S, et al. Assessment of pain behavior in a rat model of intervertebral disc injury using the CatWalk gait analysis system. Spine (Phila Pa 1976). 2013;38(17):1459–65.
32. Gabriel AF, Marcus MA, Honig WM, Walenkamp GH, Joosten EA. The CatWalk method: a detailed analysis of behavioral changes after acute inflammatory pain in the rat. J Neurosci Methods. 2007;163(1):9–16.
33. Beytemür O, Yüksel S, Tetikkurt Ü S, Genç E, Olcay E, Güleç A. Isotretinoin induced achilles tendinopathy: Histopathological and biomechanical evaluation on rats. Acta Orthop Traumatol Turc. 2018;52(5):387–91.
34. Petrosino S, Schiano Moriello A, Verde R, Allarà M, Imperatore R, Ligresti A, et al. Palmitoylethanolamide counteracts substance P-induced mast cell activation in vitro by stimulating diacylglycerol lipase activity. J Neuroinflammation. 2019;16(1):274.
35. He L, He T, Xing J, Zhou Q, Fan L, Liu C, et al. Bone marrow mesenchymal stem cell-derived exosomes protect cartilage damage and relieve knee osteoarthritis pain in a rat model of osteoarthritis. Stem Cell Res Ther. 2020;11(1):276.
36. Keith IM, Jin J, Saban R. Nerve-mast cell interaction in normal guinea pig urinary bladder. J Comp Neurol. 1995;363(1):28–36.
37. Falcone FH, Wan D, Barwary N, Sagi-Eisenberg R. RBL cells as models for in vitro studies of mast cells and basophils. Immunol Rev. 2018;282(1):47–57.

38. Khan KM, Cook JL, Kannus P, Maffulli N, Bonar SF. Time to abandon the "tendinitis" myth. Bmj. 2002;324(7338):626–7.
39. Millar NL, Hueber AJ, Reilly JH, Xu Y, Fazzi UG, Murrell GA, et al. Inflammation is present in early human tendinopathy. Am J Sports Med. 2010;38(10):2085–91.
40. Abate M, Silbernagel KG, Siljeholm C, Di Iorio A, De Amicis D, Salini V, et al. Pathogenesis of tendinopathies: inflammation or degeneration? Arthritis Res Ther. 2009;11(3):235.
41. Julius D, Basbaum AI. Molecular mechanisms of nociception. Nature. 2001;413(6852):203–10.
42. Latremoliere A, Woolf CJ. Central sensitization: a generator of pain hypersensitivity by central neural plasticity. J Pain. 2009;10(9):895–926.
43. Plinsinga ML, Brink MS, Vicenzino B, van Wilgen CP. Evidence of Nervous System Sensitization in Commonly Presenting and Persistent Painful Tendinopathies: A Systematic Review. J Orthop Sports Phys Ther. 2015;45(11):864–75.
44. Rio E, Moseley L, Purdam C, Samiric T, Kidgell D, Pearce AJ, et al. The pain of tendinopathy: physiological or pathophysiological? Sports Med. 2014;44(1):9–23.
45. Héron A, Dubayle D. A focus on mast cells and pain. J Neuroimmunol. 2013;264(1-2):1–7.
46. Kulka M, Sheen CH, Tancowny BP, Grammer LC, Schleimer RP. Neuropeptides activate human mast cell degranulation and chemokine production. Immunology. 2008;123(3):398–410.
47. Kleij HP, Bienenstock J. Significance of Conversation between Mast Cells and Nerves. Allergy Asthma Clin Immunol. 2005;1(2):65–80.
48. Matsuda H, Kawakita K, Kiso Y, Nakano T, Kitamura Y. Substance P induces granulocyte infiltration through degranulation of mast cells. J Immunol. 1989;142(3):927–31.
49. Rosa AC, Fantozzi R. The role of histamine in neurogenic inflammation. Br J Pharmacol. 2013;170(1):38–45.
50. Uder C, Brückner S, Winkler S, Tautenhahn HM, Christ B. Mammalian MSC from selected species: Features and applications. Cytometry A. 2018;93(1):32–49.
51. Liang X, Yin G, Ma Y, Xu K, Liu J, Li J. The critical role of mast cell-derived hypoxia-inducible factor-1α in regulating mast cell function. J Pharm Pharmacol. 2016;68(11):1409–16.
52. Abebayehu D, Spence AJ, Qayum AA, Taruselli MT, McLeod JJ, Caslin HL, et al. Lactic Acid Suppresses IL-33-Mediated Mast Cell Inflammatory Responses via Hypoxia-Inducible Factor-1α-Dependent miR-155 Suppression. J Immunol. 2016;197(7):2909–17.
53. Yan K, Lin Q, Tang K, Liu S, Du Y, Yu X, et al. Substance P participates in periodontitis by upregulating HIF-1α and RANKL/OPG ratio. BMC Oral Health. 2020;20(1):27.

Figures

Figure 1

Characterization of iMSCs and iMSC-sEVs. A Identification of iMSCs by flow cytometry. B Representative image of iMSC-sEVs observed by TEM. Scale bar = 100 nm. C Size distribution of iMSC-sEVs measured by nano-flow cytometer. D The expression of exosomal markers including CD9, TSG101, and CD63, but not the negative marker GM130 measured by western blot. E Evaluation of iMSC-sEVs yield in terms of particle concentration, n=3. F Evaluation of iMSC-sEVs yield in terms of protein concentration, n=3. Data were expressed as mean ± SD.

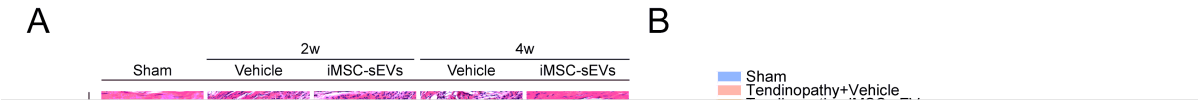

Figure 2

iMSC-sEVs alleviated the tendinopathy-related pain in a rat model. A Representative images of H&E and immunohistochemically stained tissue sections of different groups at weeks 2 and 4 after treatment. The positive area of IL-1β, IL-6 and TNF-α was visualized with DAB (brown), and nuclei were counterstained with hematoxylin (blue). Scale bar=100μm. B Quantification of H&E and immunohistochemical staining, n=5 per group. C, D Pain-related behaviors were accessed by PWT (A) and SWB (B) reversal (%) for 4 weeks after treatment, n= 3 per group. E Results of Catwalk gait analysis. Representative images of rat's paw prints in different groups at 4 weeks post-injection. For each image, the right front paw print was shown in red, the right hind paw print was shown in blue, the left front paw print was shown in purple, and the left hind paw print was shown in green. F Print area, limb swing speed, duty cycle and max contact mean intensity at 4 weeks post-injection were presented as the ratio of right /left hind values, n=5 per group. All quantitative data were expressed as mean ± SD. *P 0.05. **P 0.01. ***P 0.001. #P0.0001. ns, no significant (P0.05).

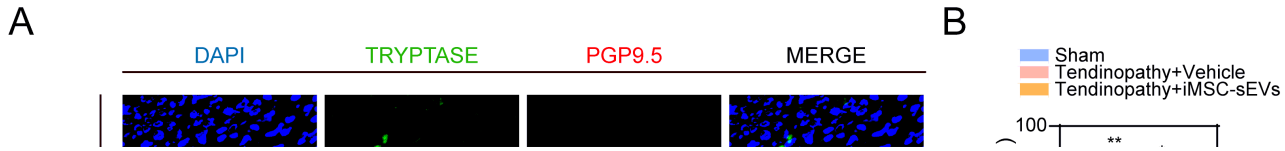

Figure 3

iMSC-sEVs inhibited mast cells infiltration and interactions with nerve fibers in the quadriceps tendon. A Representative images of double immunofluorescence staining on tendon sections for tryptase and PGP9.5. B Quantification of positive area by mean gray value, n=3 per group. C Representative images of immunohistochemical staining of NGF at weeks 2 and 4 after treatment. Positive immunostaining was visualized with DAB (brown), and nuclei were counterstained with hematoxylin (blue). Scale bar = 100μm.

D Quantification of immunohistochemical staining, n=5 per group. Data were expressed as mean ± SD. *P 0.05. **P 0.01. ***P 0.001. #P0.0001.

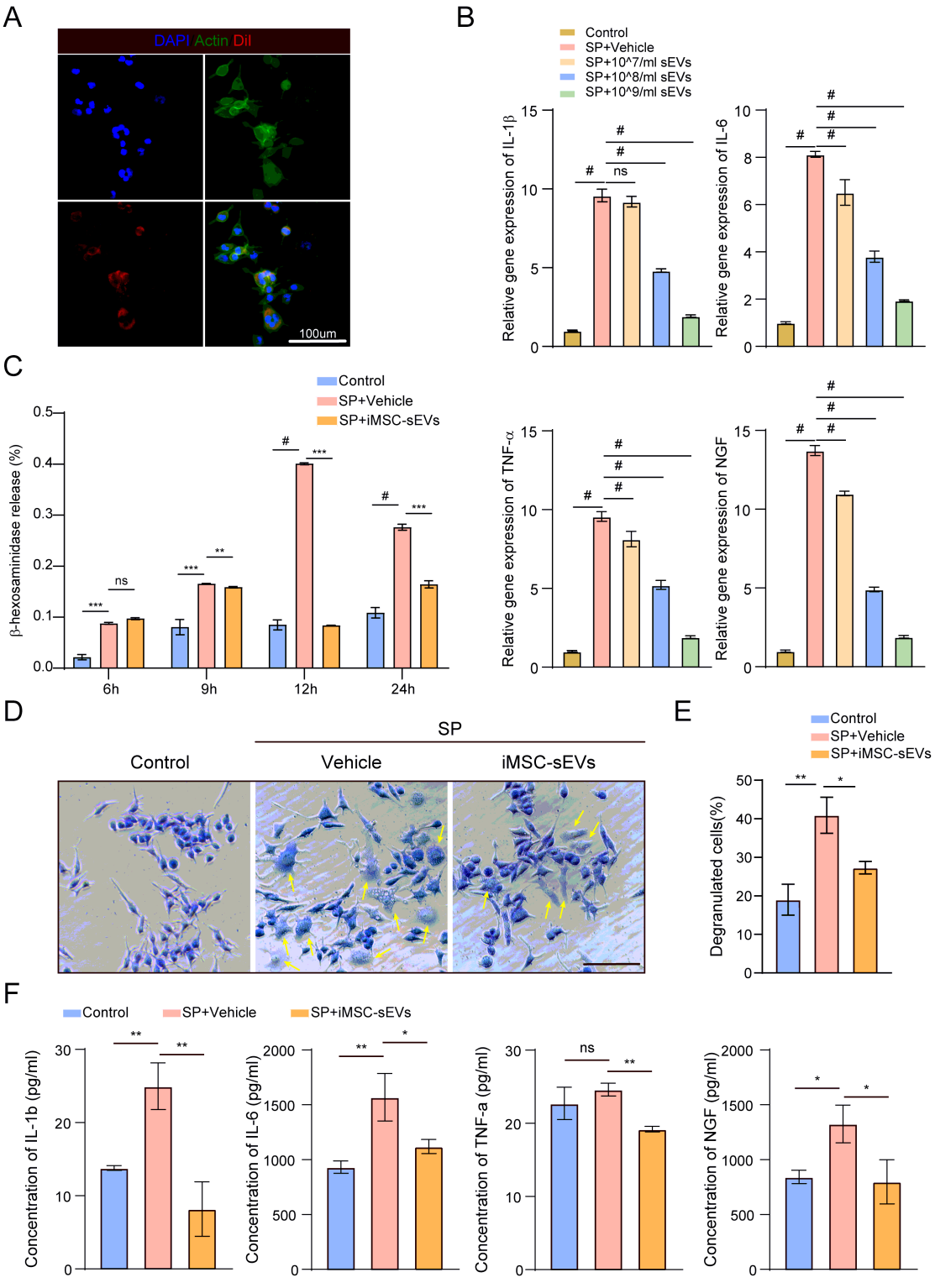

Figure 4

iMSC-sEVs restrained SP-induced degranulation of mast cells. A Representative immunofluorescence image of RBL-2H3 cells cultured with DiI labeled iMSC-sEV (red). Scale bar = 100μm. B RT-qPCR was performed to measure the expression of IL-1β, IL-6, TNF-α and NGF in RBL-2H3 cells. C The degranulation

of RBL-2H3 cells was measured by β-hexosaminidase release assay. D Toluidine blue staining was performed to measure the number of degranulated RBL-2H3 cells (yellow arrows). Scale bar = 100μm. E Quantification of the percent of degranulated mast cells. F ELISA assay was performed to detect the level of IL-1β, IL-6, TNF-α and NGF in the supernatant. Data were expressed as mean ± SD. *P 0.05. **P 0.01. ***P 0.001. #P0.0001. ns, no significant (P0.05). All experiments were repeated at least three biological replicates independently.

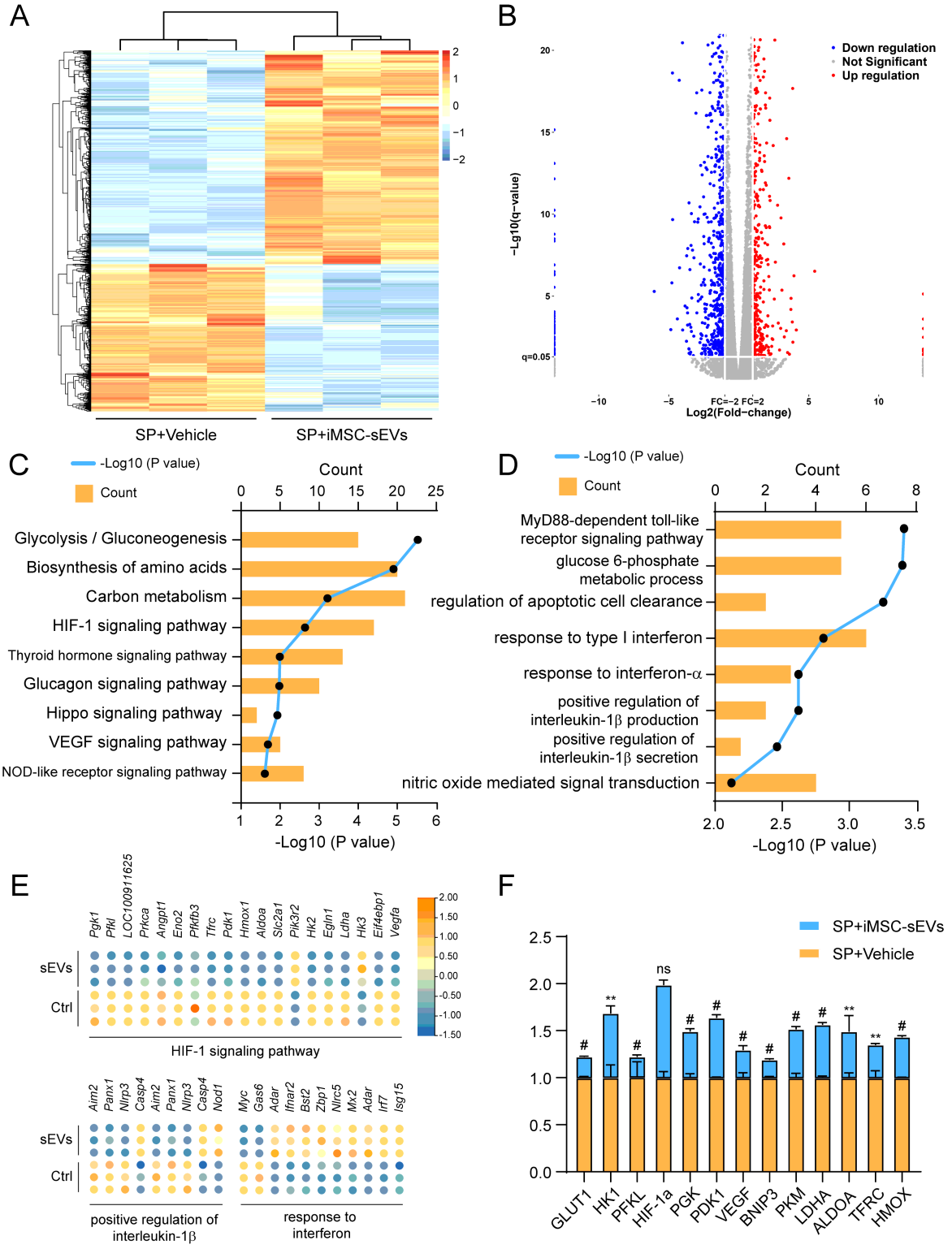

Figure 5

iMSC-sEVs modulate the gene expression pattern of mast cells. A-B Heatmap and Volcano Plot represented significant differential expression genes in RBL-2H3 cells treated with or without iMSC-sEVs. C KEGG analysis showed canonical pathways of the differentially expressed genes in RBL-2H3 cells. D GO analysis showed various biological processes of the differentially expressed genes in RBL-2H3 cells. E Heatmap represented differentially expressed genes (fold change >2) in the HIF-1 signaling pathway and biological processes like positive regulation of IL-1β and response to interferon. F RT-qPCR analysis verified the expression of HIF-1 signaling pathway-related gene in RBL-2H3 cells after iMSC-sEVs treatment. P-value was indicated as sEVs group versus vehicle group. *P < 0.05, **P < 0.01, ***P < 0.001, #P□0.0001. All experiments were repeated at least three biological replicates independently.

Supplementary Files

This is a list of supplementary files associated with this preprint. Click to download.

- Additionalfile1.pdf
- Additionalfile2.tif
- Additionalfile3.tif